Design of Minimally Invasive Method for Combustion Chamber Pressure Measurements in HTPB/N_2O Hybrid Rocket Motors

Haleigh Flaherty and Nathanial O'Neill
University of Colorado, Boulder, CO, 80309, United States

The static test fire is an essential step in characterizing the performance and behavior of aerospace propulsion systems. Measurements of the combustion chamber pressure taken during this test allow for the derivation of several important rocket characterization parameters, such as the characteristic velocity and the coefficient of thrust. Obtaining this measurement can be extremely difficult, given the extreme temperatures and pressures inside a combustion chamber. Additionally, if direct measurements are to be obtained, structural modifications are often necessary to the propulsion system, which renders the system unable be used for flight post-test. This led the team to originally investigate a non-invasive method for measuring the chamber pressure using strain gauges is discussed, but found challenges concerning the combustion chamber materials. Consequently, this paper investigates the design of a minimally invasive combustion chamber pressure measurement system for a 300 lbf thrust HTPB/N_2O hybrid rocket. This design uses a pressure transducer that is offset from the combustion chamber and connected to it via stainless steel tubing, and has proven through simulation to prevent the pressure transducer from experiencing temperatures that exceed its operational limit.

Nomenclature

$\bar{\dot{m}}$	Average mass flow rate
$\bar{F}$	Average thrust
$\bar{P}_c$	Average chamber pressure
A_t	Throat area
C^*	Characteristic velocity
C_F	Coefficient of thrust
g_c	Newton's constant
P_a	Atmospheric pressure

Contents

I. Introduction

A. Background

The pressure transducer design detailed in this paper came about through the HICKAM senior design project (**H**ybrid-rocket **I**nformation-Collection, **K**nowledgebase and **A**nalysis **M**odule) at the University of Colorado – Boulder.

The goal of this project is to create a modular, compact, and portable test stand and a performance characterization software package for hybrid rocket motors. In terms of performance related measurements, the HICKAM test stand records data on oxidizer mass flow rate, thrust, vibration, nozzle temperature, and combustion chamber pressure. With these measurements, the performance characterization software derives several performance parameters, such as: mass flow rate, total and specific impulse, nozzle throat temperature, combustion chamber temperature, fuel regression rate, oxidizer mass flux, coefficient of thrust, characteristic velocity, effective exhaust velocity, and total burn time.

B. Motivation

The direct measurement of combustion chamber pressure allows for the derivation of several important performance characterization parameters, and also provides the ability to reference our thrust measurements analytically. Chamber pressure allows the derivation of:

- Characteristic Velocity:

$$C^* = \frac{\bar{P}_c A_t g_c}{\bar{\dot{m}}} \tag{1}$$

  Where C^* is characteristic velocity, A_t is throat area, g_c is Newtons constant, and $\bar{\dot{m}}$ is the average mass flow rate.

- Coefficient of Thrust:

$$C_F = \frac{\bar{F}}{\bar{P}_c A_t} \tag{2}$$

  Where C_F is the coefficient of thrust and $\bar{F}$ is the average thrust.

- Chamber to Atmospheric Pressure Ratio

$$\frac{\bar{P}_c}{P_a} \tag{3}$$

  Where P_a is the atmospheric pressure on test day.

These parameters are important in the analysis and performance characterization of any rocket. The Characteristic Velocity, a function of propellant characteristics and combustion chamber properties independent of nozzle geometry, is used as a figure of merit when comparing different propellant combinations for combustion chamber performance. The Coefficient of Thrust provides insight into the amplification of thrust due to the expansion of gas in the divergent portion of the supersonic nozzle as opposed to the thrust that would be exerted if the combustion chamber pressure only acted over the throat area. The chamber to atmospheric pressure ratio allows for the characterization of rocket performance at a given density altitude, and will be used to approximate the nozzle exit pressure, which gives insight into the expansion behavior of the nozzle.

The usefulness of these parameters in characterizing rocket motor performance motivated team HICKAM to find a way to measure the combustion chamber pressure, despite its known difficulties. The team looked into two primary methods: measuring the chamber pressure indirectly using strain gauges and measuring the chamber pressure directly using a pressure transducer.

Both methods have their pros and cons, which can be succinctly stated as follows: the strain gauge is desirable because it is non-intrusive but undesirable because it is not a direct measurement; and the pressure transducer is desirable because it is a direct measurement, but undesirable because it is intrusive. The design decision comes down to whether or not the accuracy of the combustion chamber pressure measurement is important enough to justify the intrusive nature of using the pressure transducer.

II. Materials and Methods

A. Strain Gauge Method

The combustion chamber can be modeled as a multi-layered cylindrical pressure vessel, with, in our case, the outermost layer being carbon fiber, the middle layer being phenolic resin, and the innermost layer being the HTPB fuel grain. The following model, including figures, of determining internal pressure comes from Knut Vedeld and Havar A. Sollund.[2] Under heated, pressurized conditions, the model makes the following *a priori* assumptions:

(i) The materials in the cylinder layers are assumed to be linearly elastic, homogeneous, and isotropic.

(ii) Initial stresses and strains are disregarded.

(iii) Small displacements are assumed.

(iv) Heat is assumed to result in a uniform temperature distribution within each layer of the cylinder.

(v) Sections that are plane and perpendicular to the cylinder axis prior to the deformation are assumed to be plane and perpendicular to the cylinder axis after deformation.

(vi) The cylinders are assumed to be free to expand or contract radially.

The coordinate system is cylindrical, as seen in the following figure:

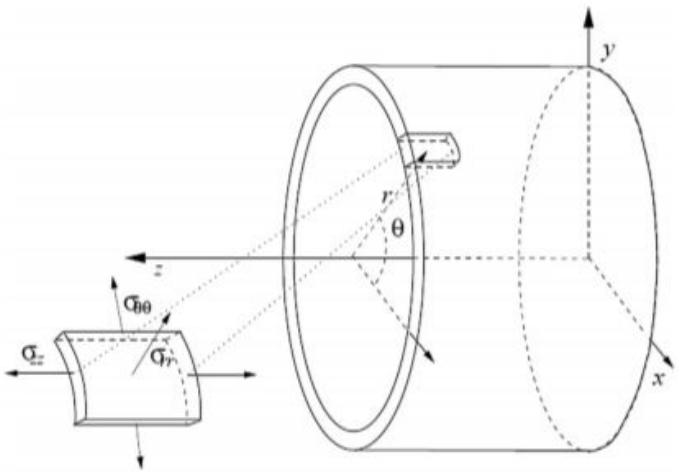

Figure 1. Coordinate System and Stress Nomenclature

Figure 2 illustrates the material properties and loading of the cylindrical pressure vessel, where, for each layer of cylinder, E_i is the Young's Modulus, ν_i is the Poisson's Ratio, α_i is the coefficient of thermal expansion, r_i is the outer radius of the $i-$th layer, p_{ext} is the external pressure, p_{int} is the internal pressure, and the temperature change across each layer is ΔT_i.

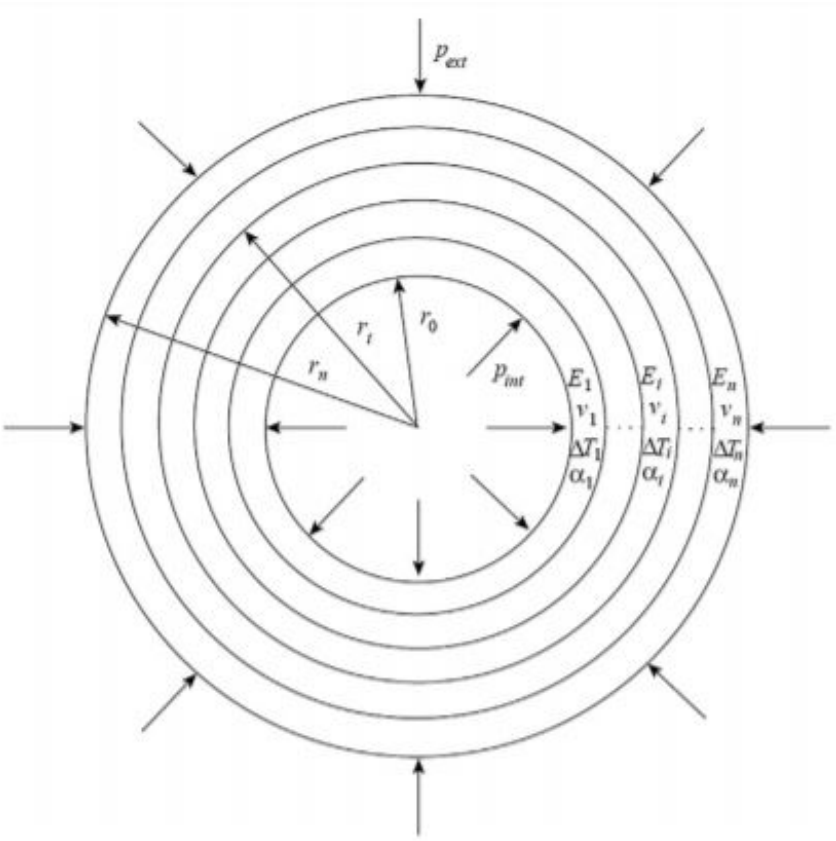

Figure 2. Caption

Let q_i denote the contact pressure between layer i and layer $(i+1)$. The boundary condition on the inner surface is then given by

$$\sigma_{rr,1} = -q_0 = -p_{int} \tag{4}$$

where the radial stress in the innermost layer is denoted by $\sigma_{rr,1}$. The boundary condition on the outer surface is then

$$\sigma_{rr,n} = -q_n = -p_{ext} \tag{5}$$

where the radial stress in the outermost layer is denoted by $\sigma_{rr,n}$.

The following algorithm can then be used to determine the lateral strain, ε_{zz}. For the sake of brevity, the equations used in the algorithm will only be listed, not derived. For a thourough derivation, see [2].

1. Initialize the model by establishing the sequences $\{\phi_i\}$, $\{\lambda_i\}$. and $\{\beta_i\}$ and $\{S_i\}$, $\{T_i\}$, and $\{\gamma_i\}$ from the following equations:

$$\phi_i = \hat{E}_i \alpha_i \Delta T_i (1 + \nu_i) \tag{6}$$

where $\hat{E}_i$ is the modified Young's Modulus given by:

$$\hat{E}_i = \frac{E_i}{(1 - 2\nu_i)(1 + \nu_i)} \tag{7}$$

$$\lambda_i = -\frac{1}{\hat{E}(1 - 2\nu_i)} = -\frac{1 + \nu_i}{E_i} \text{ and } \beta_i = \frac{1}{\hat{E}_i} \tag{8}$$

$$S_i = (\lambda_i - \beta_{i+1})\gamma_{i+1}\gamma_i + (\lambda_{i+1} - \lambda_i)\gamma_i \tag{9}$$

$$T_i = \lambda_{i+1} - \beta_i + (\beta_i - \beta_{i-1})\gamma_{i+1} \tag{10}$$

$$\gamma_{i+1} = \frac{r_i^2}{r_{i+1}^2} \tag{11}$$

2. Compute sequences $\{a_i\},\ \{c_i\}.$ and $\{d_i\}$ from the following equations:

$$a_{i+1} = \frac{(S_i - \gamma_i T_i)a_{i-1} - (S_i - T_i)a_i}{(1-\gamma_i)(\lambda_{i+1} - \beta_{i+1})} \tag{12}$$

$$c_{i+1} = \frac{(S_i - \gamma_i T_i)c_{i-1} - (S_i - T_i)c_i}{(1-\gamma_i)(\lambda_{i+1} - \beta_{i+1})} + \frac{(1-\gamma_{i+1})(\phi_i\beta_i - \phi_{i+1}\beta_{i+1})}{q_0(\lambda_{i+1} - \beta_{i+1})} \tag{13}$$

$$d_{i+1} = \frac{(S_i - \gamma_i T_i)d_{i-1} - (S_i - T_i)d_i}{(1-\gamma_i)(\lambda_{i+1} - \beta_{i+1})} - \frac{(1-\gamma_{i+1})(\nu_i - \nu_{i+1})}{q_0(\lambda_{i+1} - \beta_{i+1})} \tag{14}$$

with initial conditions $a_0 = 0,\ a_1 = 1,\ c_0 = 1,\ c_1 = 0,$ and $\ d_0 = d_1 = 0.$

3. Compute sequences $\{q_i^0\}$ and $\{\zeta_i\}$ from the following equations:

$$\zeta_i = \left(d_i - \frac{d_n}{a_n}a_i\right)q_0 \tag{15}$$

$$q_i^0 = \frac{a_i}{a_n}q_n + \left(c_i - \frac{c_n}{a_n}a_i\right)q_0 \tag{16}$$

4. Calculate the lateral strain ε_{zz} from

$$\varepsilon_{zz} = \frac{N + \sum_{i=1}^{n} r_i^2[(1-2\nu_i)(1-\gamma_i)\phi_i - 2\nu)_i(\gamma_i q_{i-1}^0 - q_i^0)]}{KL + \pi\sum_{i=1}^{n} r_i^2[E_i(1-\gamma_i) + 2\nu_i(\gamma_i\zeta_{i-1} - \zeta_i)]} \tag{17}$$

5. Calculate the contact pressures from

$$q_i = q_i^0 + \zeta_i\varepsilon_{zz} \tag{18}$$

6. Calculate A_i and C_i:

$$\frac{A_i}{r_i^2} = \frac{\gamma_i(q_i - q_{i-1}}{1-\gamma_i} \tag{19}$$

$$C_i = \frac{(\gamma_i q_{i-1})}{(1-\gamma_i)} + \mu_i \tag{20}$$

where μ_i is given by:

$$\mu_i = \phi_i - \hat{E}_i\nu_i\varepsilon_{zz} \tag{21}$$

7. The radial displacement field can then be obtained from:

$$u_{r,i} = \lambda_i\frac{A_i}{r} + \beta_i C_i r \tag{22}$$

$$u_{\theta,i} = 0 \tag{23}$$

$$u_z = C_z\frac{z}{L} = \varepsilon_{zz}z \tag{24}$$

$$\begin{bmatrix}\sigma_{rr,i}\\ \sigma_{\theta\theta,i}\\ \sigma_{zz,i}\end{bmatrix} = \begin{bmatrix}\frac{A_i}{r^2} + C_i - \mu_i\\ -\frac{A_i}{r^2} + C_i - \mu_i\\ 2\nu_i C_i + \hat{E}_i(1-\nu_v)\varepsilon_{zz} - \phi_i\end{bmatrix} \tag{25}$$

Recall that the boundary condition for the innermost layer is given by

$$\sigma_{rr,1} = -q_0 = -p_{int} \tag{26}$$

Given that the strain gauges would provide direct measurements of ε_{zz}, we can then work backwards to solve for the initial boundary condition $\sigma_{rr,1} = -p_{int}$ and back out the internal pressure.

B. Pressure Transducer Method

A pressure transducer cannot be used in a traditional sense to directly measure the combustion chamber pressure due to the nature of the combustion chamber environment – the extreme heat of combustion would rapidly destroy the pressure transducer, likely causing mechanical failure and spontaneous, un-scheduled disassembly of the rocket. As this is obviously undesirable, one must get creative in how they implement the pressure transducer to take measurements of the pressure. The HICKAM team addressed this issue by going through several design iterations of what we call an "offset design".

As the name would imply, the offset design distances the pressure transducer from the combustion chamber and attaches the two together via some sort of tubing, utlizing the offset to prevent excessive heat transfer that would destroy the pressure transducer. Figure 3 shows the HICKAM test article, a N_2O/HTPB hybrid motor designed by a previous year's senior project (MaCH SR-1 2005-2006).

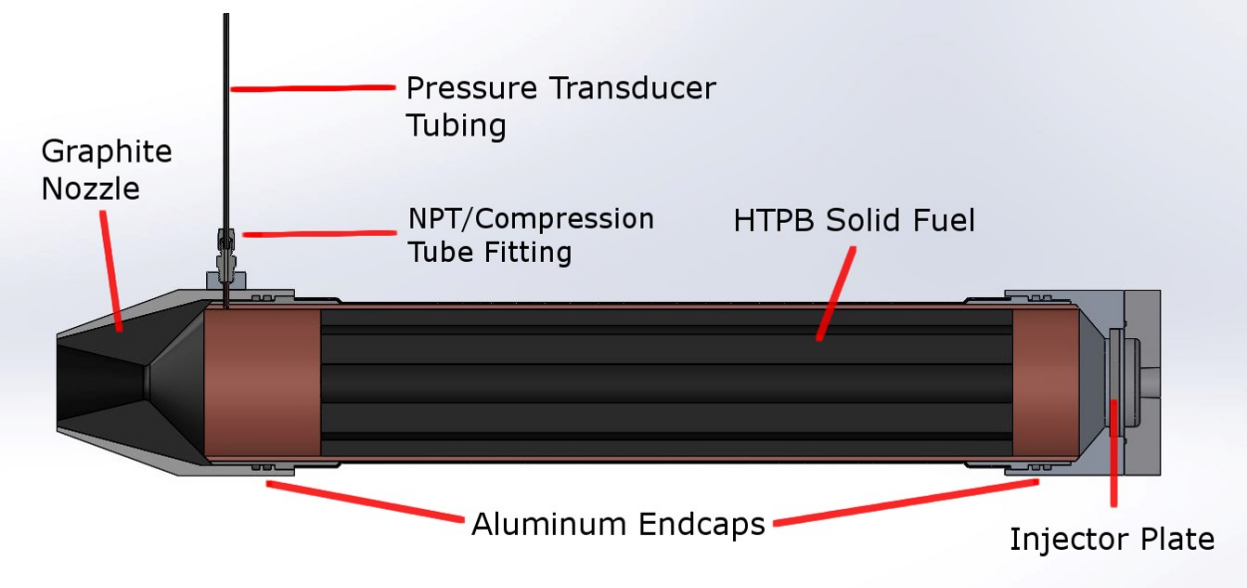

Figure 3. Rocket Motor with Pressure Transducer Attachment

Zooming in, further detail of the design can be seen Figure 4

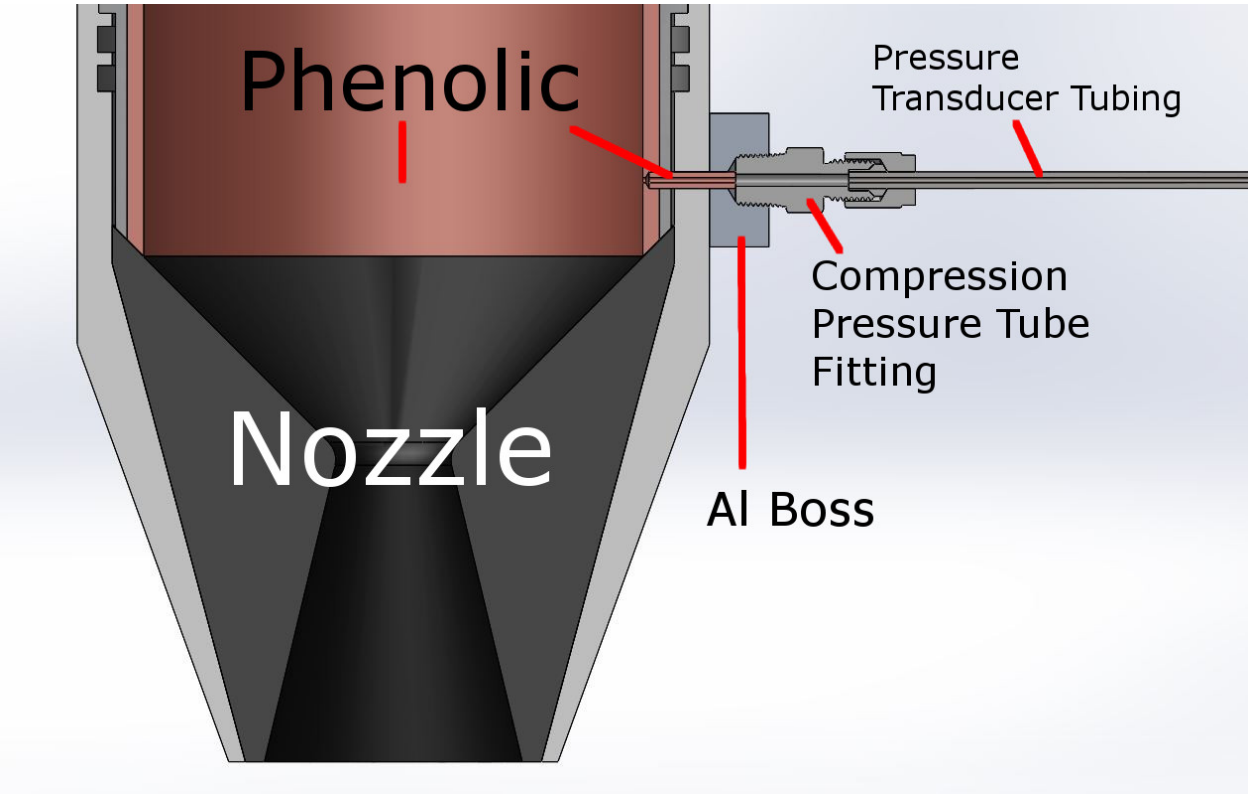

Figure 4. Zoom into nozzle section

To provide even further clarity, we can zoom in once more:

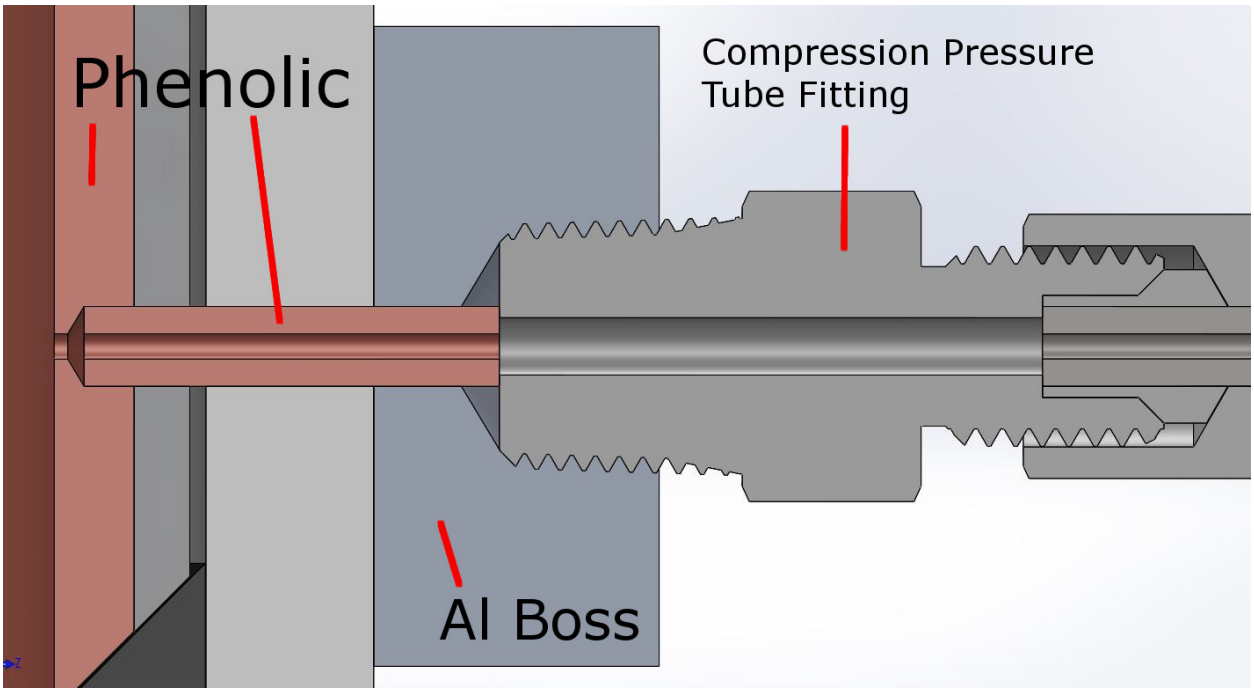

Figure 5. Zoom into attachment

The main elements of this design are the NPT/Compression fitting, the small phenolic cylinder in between

the fitting and the combustion chamber, and the aluminum boss securing the NPT/Compression fitting to the nozzle housing. The design considerations and decisions surrounding these elements are summarized in the following:

- NPT/Compression Fitting: One of the earlier designs implemented straight threads to connect the pressure transducer tubing to the test article; however, straight threads are not good at sealing, meaning that combustion products were likely to escape during the hot fire. This would cause direct contact between the combustion products and the stainless steel and aluminum of the nozzle housing, likely melting these elements and causing a test article failure. Thus, the team opted for an NPT/Compression fitting to secure the pressure transducer tubing to the rocket, as an NPT fitting is traditionally used to provide a strong seal in high pressure environments.

- Phenolic Cylinder: The radiative emissivity of combusting gases is very high, with values estimated to be approximately 0.90 or higher. Any exposed aluminum or stainless steel would see extreme radiative heat transfer and likely melt. Additionally, although phenolic has an extremely low conductive heat transfer coefficient, the temperature near the phenolic reaches temperatures exceeding $1000C°$. The combined effect of these two modes of heat transfer motivated the team to insert a small insulator in between the pressure transducer fitting to increase the amount of insulation between the heat of combustion and the temperature sensitive metallic components.

- Aluminum Boss: The reasoning behind this component is simple: there is not much material for threads to grab onto in the nozzle housing, tapping into the nozzle housing would reduce the length of the phenolic insulator, thus decreasing its effectiveness. Additionally, as the temperature increases closer to the combustion chamber, the higher the thermal deformation will be, thus increasing the chance of seal failure. The aluminum boss allows for more threads, gives the phenolic insulator a larger allowable length, and decreases the temperature that the threads will be exposed to.

A major consideration in the design of this attachment was the intrusiveness of it – the design should accomplish its objective without interfering with the combustion process inside the combustion chamber. This design follows standard engineering practice for pressure measurements, with a pressure hole (the through-hole that exists uninterrupted between the pressure transducer and the combustion chamber) of diameter 0.04 in. Additionally, the design should not require extensive modifications that could compromise the structural integrity of the rocket.

To validate this design, the team ran a transient thermal simulation in ANSYS to ensure that the temperature of the stainless steel tubing that connects to the pressure transducer did not exceed the maximum operating temperature of the pressure transducer ($100°C$). The thermal simulation was then coupled with a transient structural simulation to estimate the deformation cause by the combined effects of the temperature and pressure of combustion. The thermal model took into account radiative and convective heat transfer and was run with an adiabatic flame temperature of 3200 $°C$, which is about $200°C$ higher than the adiabatic flame temperature of HTPB and N_2O. The mechanical simulation was run with a combustion chamber pressure of 500 $psi = 3.447 \times 10^6$ Pa, which is approximately 125 psi higher than that expected for the MaCH SR-1 test article.

Note that the node limit in ANSYS Student prevented the team from running a simulation on the whole rocket, restricting us to simulating the nozzle end only, and that values for the convective film coefficient and the radiative emissivity were approximated for the simulation due a complete lack of case specific values. The convective film coefficient was approximated to to be $1,000$ $[W/m\ °C]$ and the emissivity was approximated as .93. Also note that, once again due to the node limit in ANSYS Student, the NPT/Compression fitting was approximated by a cylinder of the same material and equivalent dimension. The transient thermal simulation then produced the following results:

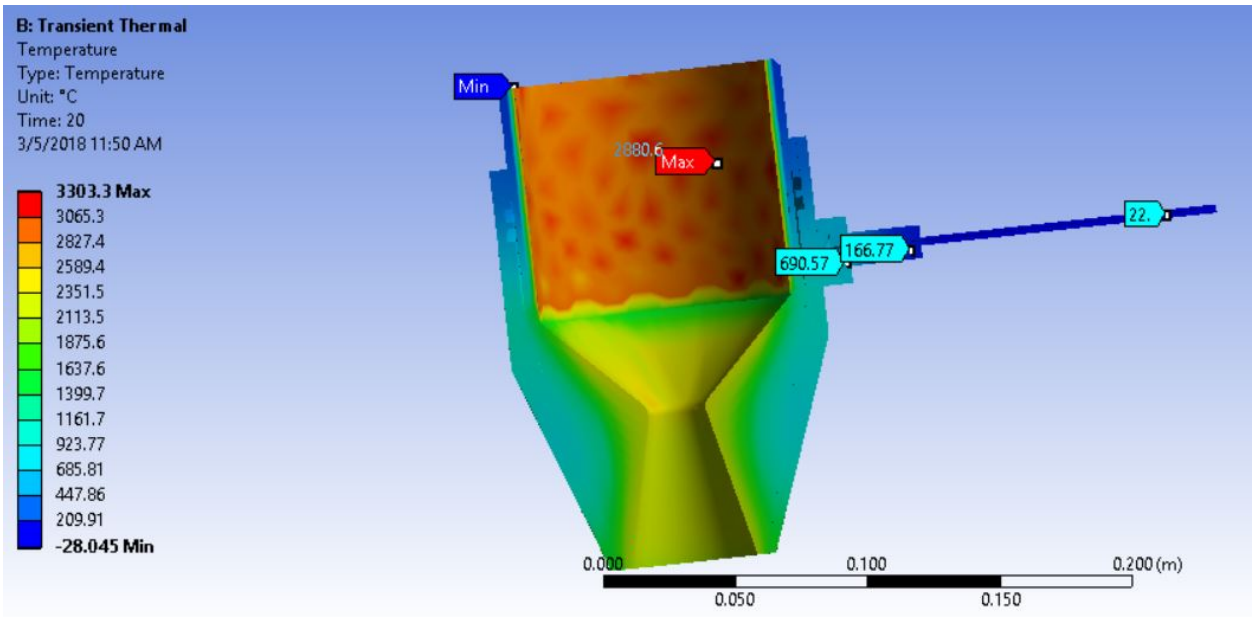

Figure 6. Results from ANSYS Thermal Simulation.

Zooming into the pressure transducer attachment:

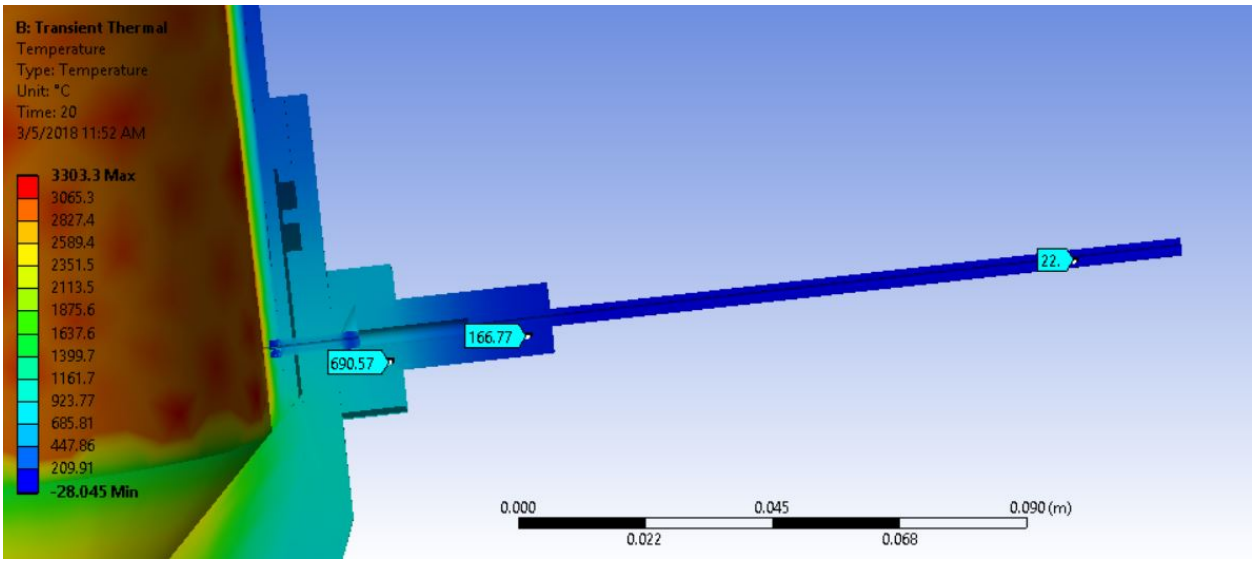

Figure 7. Results from ANSYS Thermal Simulation.

From the thermal simulation, we see that the stainless steel tubing or NPT/Compression (both 316 stainless steel) fitting never exceed their maximum service temperature of approximately 1000 $^{\circ}C$. Additionally, we see that after approximately 5 $in.$ of stainless steel tubing, the temperature is back to ambient. The structural simulation was set up with fixed supports around the aft section of the nozzle to imitate the carbon fiber wrapping that would limit expansion, as well as a frictionless support that the nozzle throat. Note that the nozzle support was enforced due to the assumption that throat regression can be considered negligable (for the purposed of this model).

Pressure values were then calculated and enforced in the model based on the assumption that the sonic conditions occur at the throat of the nozzle. The chamber pressure is 500 psi; the pressure between the chamber and nozzle throat is 378.8 psi; the throat (sonic) pressure is 275.6 psi; and the pressure downstream of the nozzle is 144.3 psi. To calculate these values, the sonic pressure was first found. From this value, the

pressures upstream and downstream of the nozzle throat were interpolated from the chamber and atmospheric pressures (assuming perfectly expanded nozzle), respectively, and assumed to be constant along the given surface area.

After coupling the simulations, it was run. The simulation produced deformations that fell well within acceptable values, providing confidence that the the seal will maintain its integrity and that the temperature will not exceed any unsafe values at any point in the attachment.

III. Discussion and Conclusions

One additional complication with the pressure transducer method is found within testing and validation. The nature of models requires for them to be validated, but the only environment in which the models can be truly validated is during the hot fire – at which time the design would ideally be validated. Hydrostatic tests may be useful as a method of checking the seal quality of the attachment, but given that the total area exposed to pressure in the axial direction of the stainless steel tubing (the direction in which thread shear force occurs) is *very* small, there is no concern of the force experienced by the attachment (it is on the order of several lbf) causing mechanical failure. A thermal test may be done to validate the heat transfer models, but such a test cannot fully validate the design. It is not the static loading nor the thermal loading that is of concern, but the coupled effect of both of them together. At least within the scope of this project, such an environment can only be achieved with a hot fire test.

Should attachment failure occur during hot fire, an analysis of the failure modes may provide insight into what went wrong with the design and which parts of the model were not accurately predicting the structural behavior. For example: if the threads shear close to the base, then the model did not sufficiently take into account the weakening of the threads due to an increase in temperature; if the threads shear close to the middle or near the tips, then the model did not sufficiently predict the thermal expansion of the threaded connection – in such an event, combustion products likely began to escape as the seal integrity diminished, causing a rapid increase in temperature that ended in thread failure; or if combustion products begin to escape during the hot fire, the design did not provide an adequate seal.

Despite these complications, the HICKAM team decided to move forward with the pressure transducer method of measuring the combustion chamber pressure for two primary reasons: the difficulty in implementing the strain gauge method far exceeded that of the pressure transducer method, and the nature of project demands accurate pressure measurements to characterize rocket motor performance.

The strain gauge method presents extraordinary complexity in the case of a hybrid (or solid) rocket motor due to the changing thickness of the fuel grain, which acts as the innermost layer of the pressure vessel. Moreover, not only is the thickness of the fuel grain changing with time, its changing non-linearly in the radial direction and at different rates along the axial direction, as seen in Figure 8.[3]

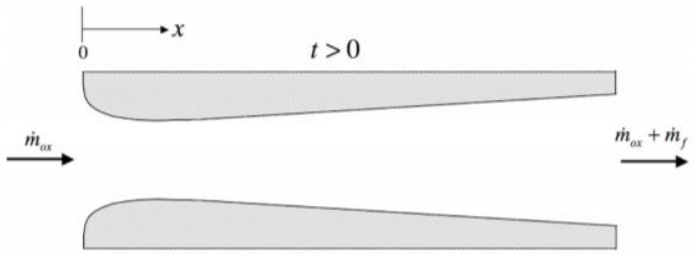

Figure 8. Hybrid Motor Fuel Regression vs. Combustion Chamber Length

Such behavior would demand the implementation of an additional model that predicts the fuel regression profile of the solid fuel and implements that in the multi-layer cylindrical pressure vessel model. Additionally, one must take into account the mechanical constraints of the combustion chamber endcaps restricting the expansion of the pressure vessel, as well as the deformative behavior of a layered composite like carbon fiber. Evidently, one could not seriously hope to derive even remotely accurate measurements from such a model.

Although the idea of measuring combustion chamber pressure with strain gauges is very appealing given the non-intrusive and robust nature of the measurement, it is just not a practical method for measuring the

combustion chamber pressure in hybrid (or solid) rocket motors.

The design detailed throughout this paper provides a minimally intrusive method of gathering accurate, direct combustion chamber pressure measurements. Despite the downsides of this measurement method (i.e. the necessity to permanently modify the rocket structure), the HICKAM team believes it to be the superior method when compared to the strain gauge method.

Appendix

References

[1]Vedran Alagic, Kendra Kilbride, Hwapyong Ko, Jacob LaBonte, Brent Lewis, David Owen, Adam McNeill, Richard Rieber, Richard Rodriguez, Alex Romanov, "MaCH-SR1 Spring 2006 Final Report," Past Senior Projects Archive, University of Colorado Boulder, Boulder, CO, 2006 (Unpublished).

[2]Knut Vedeld and Hvar A. Sollund. "Stresses in heated pressurized multi-layer cylinders in generalized plane strain conditions," *International Journal of Pressure Vessels and Piping, Volumes 120121, AugustSeptember 2014, Pages 27-35.*

[3]Author Unknown, "Chapter 11: Hybrid Rockets." https://web.stanford.edu/ cantwell/AA283_Course_Material/AA283 _Course_Notes/AA283_Aircraft_and_Rocket _Propulsion_Ch_11_BJ_Cantwell.pdf [Accessed 16 Mar. 2018]